Nonlocal Smeared Cracking Model for Concrete Fracture

By Zdeněk P. Bažant,[1] Fellow ASCE, and Feng-Bao Lin,[2] Associate Member, ASCE

Abstract: The classical smeared cracking model widely used in finite-element analysis of concrete and rock cannot describe the size effect experimentally observed in brittle failures and exhibits spurious mesh sensitivity with incorrect convergence to zero energy dissipation at failure. The crack band model circumvents these deficiencies but has limitations with respect to mesh refinement, shear locking on zig-zag crack bands, and directional bias of the mesh. It is shown that all of these problems can be avoided by a nonlocal generalization, in which the damage that characterizes strain softening is considered to be a function of the spatial average of the positive part of the maximum principal strain. Two alternatives are presented: (1) Smeared cracking whose direction is fixed when cracks start to form; and (2) smeared cracking whose orientation rotates with the maximum principal strain. Furthermore, fracture tests on specimens of various sizes are analyzed by finite elements. It is shown that the model correctly reproduces the experimentally observed size effect and agrees with Bažant's size effect law. Orthogonal and slanted meshes are shown to yield approximately the same cracking zones and propagation directions. The model is easily programmed and computationally more efficient than the corresponding local version.

Introduction

The cracking in concrete structures has widely been modeled in finite-element analysis by adjustments of material stiffness. This approach, called smeared cracking, was proposed by Rashid (1968), refined by many others, and has provided good results in many practical applications (Bažant 1986; Bc Borst 1984; Dc Borst and Nauta 1984, 1985; "Finite element analysis of reinforced concrete" 1982; Hand et al. 1973; Lin and Scordelis 1975; Suidan and Schnobrich 1973; Yuzugullu and Schnobrich 1973). Nevertheless, problems were also encountered. In 1974, it was shown by stability analysis of strain softening (Bažant 1976) and demonstrated numerically (Bažant and Cedolin 1979, 1980; Bažant and Oh 1983; Cedolin and Bažant 1980; Darwin 1985; De Borst 1984) that the classical smeared cracking model is unobjective, exhibiting spurious mesh sensitivity and convergence to an incorrect failure mode with zero energy dissipation. As a related deficiency, the numerical results obtained with geometrically similar meshes exhibit no size effect, while test results for brittle failures of concrete structures as well as fracture specimens show a pronounced size effect (Bažant 1984, 1986; Bažant and Pfeiffer 1987). As a remedy, Bažant proposed in 1974 a model (Bažant 1976), later called the crack band model (Bažant and Oh 1983, 1984), whose distinguishing characteristic is that no finite element is allowed to become smaller than a certain characteristic length w_c which is a material property and is related to the size of inhomogeneity in the material. Extended to de-

[1]Prof., Dept. of Civ. Engrg., Northwestern Univ., Evanston, IL 60208.
[2]Asst. Prof., Dept. of Civ. and Envir. Engrg., Polytechnic Univ., Brooklyn, NY 11201.

Note. Discussion open until April 1, 1989. To extend the closing date one month, a written request must be filed with the ASCE Manager of Journals. The manuscript for this paper was submitted for review and possible publication on September 2, 1987. This paper is part of the ***Journal of Structural Engineering***, Vol. 114, No. 11, November, 1988. ©ASCE, ISSN 0733-9445/88/0011-2493/$1.00 + $.15 per page. Paper No. 22936.

scribe progressive cracking characterized by gradual strain softening (Bažant and Oh 1983), the crack band model was shown to agree with all of the basic experimental data from concrete or rock fracture testing.

An alternative is to model concrete fractures as interelement line cracks, as proposed by Ngo and Scordelis (1967). Adapting to concrete Dugdale and Barrenblatt's ductile fracture model (Bažant 1986), Hillerborg et al. (Hillerborg 1985; Hillerborg et al. 1976) recognized that the line crack must be endowed with a softening cohesion zone near the crack tip, in order to obtain agreement with fracture test results. This approach was later found to be essentially equivalent to the crack band model, except for the case of many closely spaced parallel fractures. Although Ingraffea et al. (Ingraffea 1985; Ingraffea et al. 1985; Ngo and Scordelis 1967) succeeded in implementing line cracks (interelement cracks) in large finite-element programs, this approach seems generally more difficult to program than the smeared cracking. It might also be less realistic since no condition on minimum admissible crack spacing is used in this model but appears to be required for objectivity. Furthermore, it has not been demonstrated that remeshing with extreme mesh refinements at crack tip, as used in this approach, introduces no bias for the direction of crack progagation.

The existing crack band model nevertheless suffers with several disadvantages: (1) Refinement of the mesh in which the cracking zone width is subdivided into more than one element is not permitted, for reasons of objectivity; (2) in the case of zig-zag crack band propagation through the mesh, one needs to introduce some mathematical artifices to prevent spurious locking of the rugged opposite sides of the crack band (Droz 1987) (the same problem exists for shear bands); (3) the mesh, typically a square mesh, inevitably introduces a certain degree of directional bias for the crack propagation, favoring propagation along the mesh lines or along the diagonals of the mesh, and suppressing propagation directions of small inclination with regard to the mesh line (Marchertas et al. 1982; Pan et al. 1983; 1984); and (4) possible variations of the cracking zone width, which would cause variations in the specific energy required for propagation, cannot be taken into account (neither can this be done for the discrete crack models).

The foregoing disadvantages can be eliminated by adopting a nonlocal continuum approach (Eringen and Edelen 1972) whose application to strain softening was proposed by Bažant et al. (1984). The objective of the present study is to introduce a new, simple version of the nonlocal approach whose general idea was discovered recently (Bažant et al. 1987; Bažant and Pijaudier-Cabot 1987, 1988; Pijaudier-Cabot and Bažant 1986, 1987). The idea is that the nonlocal treatment should be applied only to those variables which cause strain softening, while the other variables, especially the elastic strain, should be local. In this form of nonlocal approach, the differential equations of equilibrium with the boundary conditions retain their standard form, no extra boundary conditions need to be introduced, the continuity requirements for finite elements remain the same as for the local formulation, and spurious zero-energy periodic instability modes, which caused problems for the original nonlocal formulation (Bažant et al. 1984), do not exist.

Alternative I. Cracking of Fixed Direction

In two dimensions, the crack band model may be characterized by the stress–strain relation:

$$\begin{Bmatrix}\epsilon_{11}\\ \epsilon_{22}\\ \gamma_{12}\end{Bmatrix} = \begin{bmatrix}C_{1111} & C_{1122} & 0\\ C_{2211} & C_{2222} & 0\\ 0 & 0 & C_{1212}/\beta\end{bmatrix}\begin{Bmatrix}\sigma_{11}\\ \sigma_{22}\\ \sigma_{12}\end{Bmatrix} + \begin{Bmatrix}\epsilon^f\\ 0\\ 0\end{Bmatrix} \quad \ldots\ldots (1)$$

in which ϵ^f is the fracturing strain; ϵ_{11}, ϵ_{22}, and γ_{12} are the normal strains and the shear angle ($\gamma_{12} = 2\epsilon_{12}$); σ_{11}, σ_{22}, and σ_{12} are the normal and shear stresses; C_{1111}, C_{2222}, C_{1212}, and C_{1122} are the initial elastic compliances; and the numerical subscripts refer to the cartesian coordinates x_1 and x_2. Assuming isotropy, we have $C_{1111} = C_{2222} = 1/E'$, $C_{1122} = C_{2211} = \nu'/E'$, $C_{1212} = 2(1 + \nu)/E$, in which for plane stress $E' = E$, $\nu' = \nu$, and for plane strain $E' = E/(1 - \nu^2)$, $\nu' = \nu/(1 - \nu)$.

The cracks are assumed to be all parallel and normal to the axis x_1. As the first alternative of the smeared cracking model, we introduce the classical hypothesis that, at the time the cracks start to form, the direction of the cracks (i.e., of the axis x_1) is fixed as normal to the maximum principal stress σ_t at that instant and remains constant afterwards. If σ_t does not rotate, σ_{12} remains zero; however in general σ_t may rotate, and in that case one must take into account the shear stiffness due to aggregate interlock on rough crack surfaces. This is done by multiplying the shear compliance C_{1212} with an empirical coefficient β, called the shear retention factor, as proposed (for sudden cracking) by Schnobrich et al. (Hand et al. 1973; Suidan and Schnobrich 1973; Yuzugullu and Schnobrich 1973) and others (Lin and Scordelis 1975). More realistically, the coefficient β could be assumed to vary according to the rough crack model (Bažant and Gambarova 1981).

It has been shown (Bažant and Oh 1983) that Eq. 1 is equivalent to the equation:

$$\begin{Bmatrix}\epsilon_{11}\\ \epsilon_{22}\\ \gamma_{12}\end{Bmatrix} = \begin{bmatrix}C_{1111}/(1 - \omega) & C_{1122} & 0\\ C_{2211} & C_{2222} & 0\\ 0 & 0 & C_{1212}/\beta\end{bmatrix}\begin{Bmatrix}\sigma_{11}\\ \sigma_{22}\\ \sigma_{12}\end{Bmatrix} \quad \ldots\ldots (2)$$

in which the normal stiffness C_{1111} in the direction normal to the cracks is reduced by the coefficient $1 - \omega$, where ω represents what is known in continuum damage mechanics as damage and may be regarded as the cracked area fraction; $\omega = 0$ corresponds to the initial state of no cracking (zero damage); and $\omega = 1$ corresponds to the final state of complete cracking (complete damage). Comparing Eqs. 1 and 2, we note that $\epsilon^f = [\omega C_{1111}/(1 - \omega)]\sigma_{11}$.

Although in general the evolution of damage may be described in the form $\dot{\omega} = F(\omega, \epsilon)$, one may simply assume that, for monotonic loading, $(1 - \omega)^{-1} = \phi(\epsilon_{11}) =$ function that characterizes the cracking in the material. Assuming unloading and reloading to follow the secant modulus (which is the basic hypothesis of continuum damage mechanics), we may write:

$$\text{If } \epsilon_{11} \geq \epsilon_{max} \text{ and } \Delta\epsilon_{11} \geq 0: \quad \frac{1}{1 - \omega} = \phi(\epsilon_{11}); \quad \text{otherwise } \Delta\epsilon = 0 \ldots\ldots (3)$$

in which Δ refers to a small increment over the loading step; and ϵ_{max} denotes the maximum strain ϵ_{11} attained in all of the preceding steps. The assumption of secant unloading is of course a simplification, and various refinements

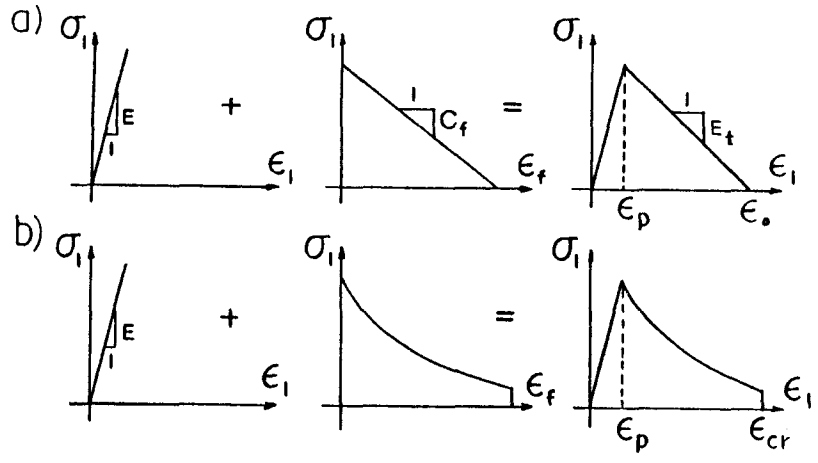

FIG. 1. (*a*) Linear and (*b*) Exponential Strain Softening

with more complex unloading rules may be introduced.

A widely used assumption has been a triangular stress–strain diagram for uniaxial loading [Fig. 1(*a*)]. In this case,

$$\text{for } \epsilon_{11} \le \epsilon_p: \quad \phi(\epsilon_{11}) = 1$$

$$\text{for } \epsilon_p < \epsilon_{11} < \epsilon_0: \quad \phi(\epsilon_{11}) = \frac{E}{E_t}\frac{\epsilon_{11}}{\epsilon_0 - \epsilon_{11}} \qquad (4)$$

$$\text{for } \epsilon_{11} \ge \epsilon_0: \quad \phi(\epsilon_{11}) = 0$$

in which ϵ_p is the strain at peak stress (cracking initiation); and ϵ_0 is the strain when the stress is reduced to zero (full cracking).

Recently various experimental evidence indicates that it is more realistic to assume a strain-softening curve with a steep initial decline followed by an extended tail. In that case, one may use

$$\text{for } \epsilon_{11} \le \epsilon_p: \quad \phi(\epsilon_{11}) = 1$$

$$\text{for } \epsilon_p < \epsilon_{11} < \epsilon_{cr}: \quad \phi(\epsilon_{11}) = \frac{E}{f_t'}\epsilon_{11}e^{\alpha(\epsilon_{11}-\epsilon_p)} \qquad (5)$$

$$\text{for } \epsilon_{11} \ge \epsilon_{cr}: \quad \phi(\epsilon_{11}) = 0$$

in which we introduce a certain critical (or maximum) strain ϵ_{cr} [Fig. 1(*b*)] that may not be exceeded in strain softening. Our introduction of ϵ_{cr} differs from the existing practice in which the strain-softening curve has been assumed to approach the strain axis in a continuous descent. Recent micromechanics analysis of crack ligament tearing (Bažant 1987), however, indicated that, for strain softening, there should exist a certain maximum strain after which the stress–strain diagram should exhibit a snapback, i.e., revert to a positive slope. The value of ϵ_{cr} has been considered to correspond to a point where $\sigma_{11} = 0.05\ \sigma_p$. This ϵ_{cr} value is so large that it has never been reached in the present computations.

Nonlocal Generalization with Local Elastic Strain

The nonlocal continuum is a continuum for which at least some variables are defined by spatial averaging. As discovered in Bažant and Pijaudier-Cabot (1987, 1988) and Pijaudier-Cabot and Bažant (1987), only those variables that cause strain softening should be considered as nonlocal. In the present context, this means that the damage ω should be made nonlocal. This is accomplished by specifying it as a function of the average (nonlocal) strain, which is defined by spatial averaging as follows:

$$\bar{\epsilon}_{11}(\mathbf{x}) = \frac{1}{V_r(\mathbf{x})}\int_V \alpha(\mathbf{s}-\mathbf{x})\langle\epsilon_{11}(\mathbf{s})\rangle dV = \int_V \alpha'(\mathbf{x},\mathbf{s})\langle\epsilon_{11}(\mathbf{s})\rangle dV \qquad (6)$$

in which

$$V_r(\mathbf{x}) = \int_V \alpha(\mathbf{s}-\mathbf{x})dV, \quad \alpha'(\mathbf{x},\mathbf{s}) = \frac{\alpha(\mathbf{s}-\mathbf{x})}{V_r(\mathbf{x})} \qquad (7)$$

The overbar is a label for the nonlocal variables, V = volume of the entire body, $\alpha(\mathbf{x})$ = given weighting function which is treated as a material property, and $\mathbf{s}$ = general coordinate vector [Fig. 2(*b*)]. V_r has approximately but not exactly the same meaning as the representative volume in the statistical theory of heterogeneous materials. The pointed brackets $\langle\ \rangle$ denote the positive part of the variable; i.e. $\langle\epsilon\rangle = \epsilon$ if $\epsilon > 0$ and 0 if $\epsilon \le 0$.

The weighting function could be defined as uniform ($\alpha = 1$) over volume V_r represented as a circle in two dimensions, and zero outside V_r. However, it has been experienced that the calculations converge better if the weighting function is smooth. A suitable choice is the normal (Gaussian) distribution function:

$$\alpha(\mathbf{x}) = e^{-(k|\mathbf{x}|/l)^2} \qquad (8)$$

in which k is a constant whose value is $k = 2$ for the case of two dimensions; $|\mathbf{x}|^2 = x^2 + y^2$; and l is the characteristic length of the material, which may be interpreted as the radius of a circle on which the uniform distribution $\alpha = 1$ has the same volume as the normal distribution function extending to infinity in the plane.

If the body is finite, the normal distribution function obviously extends beyond the boundary. This is handled by deleting the region outside the body

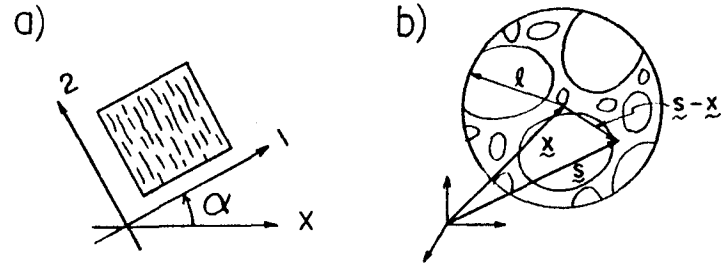

FIG. 2. (*a*) Distributed Cracking of Single Orientation; and (*b*) Representative Volume of Material Compared to Aggregate Size

from the integration domain V, both for the calculation of the average (Eq. 6) and for the calculation of the representative volume (Eq. 7). This fact causes V_r to depend on location $\mathbf{x}$.

In finite-element calculations, the integrals in Eqs. 6 and 7 are approximately evaluated as finite sums over all the integration points of all the elements in the structure. However, the integration points whose distances from the point $\mathbf{x}$ exceed approximately $2l$ may be omitted since for them the value of α is negligible.

In preliminary calculations, Eq. 6 did not involve the symbol $\langle\ \rangle$, i.e., the averaging was made directly over ω rather than over $\langle\epsilon_{11}\rangle$. However, this had to be abandoned since ω does not grow for $\epsilon_{11} > \epsilon_0$, which meant that the average of ω could never attain full damage ($\omega = 1$) unless the damage was the same in all of the elements. Therefore, the nonlocal damage $\bar{\omega}$ is considered to be a function of the nonlocal normal strain $\bar{\epsilon}_{11}$, i.e.,

$$(1 - \bar{\omega})^{-1} = \phi(\bar{\epsilon}_{11}) \quad \ldots\ldots (9)$$

The nonlocal constitutive equation with local strain takes the form:

$$\begin{Bmatrix} \epsilon_{11} \\ \epsilon_{22} \\ \gamma_{12} \end{Bmatrix} = \begin{bmatrix} C_{1111}/(1-\bar{\omega}) & C_{1122} & 0 \\ C_{2211} & C_{2222} & 0 \\ 0 & 0 & C_{1211}/\beta \end{bmatrix} \begin{Bmatrix} \sigma_{11} \\ \sigma_{22} \\ \sigma_{12} \end{Bmatrix} \quad \ldots\ldots (10)$$

In matrix form, Eq. 10 may be written as $\boldsymbol{\sigma}' = \mathbf{D}'\boldsymbol{\epsilon}'$ in which $\mathbf{D}' = \mathbf{C}'^{-1}$ and $\mathbf{C}'$ = compliance matrix, referring to the local coordinate axes which are set to lie normal to the maximum principal strain direction when the strain softening begins. In finite-element programs, Eq. 10 must of course be transformed to the global coordinates, taking the form $\boldsymbol{\sigma} = \mathbf{D}\boldsymbol{\epsilon}$, in which $\mathbf{D} = \mathbf{T}^T\mathbf{D}'\mathbf{T}$ and $\mathbf{T}$ = rotation matrix.

In each loading step, the finite-element calculations utilize the direct stiffness iteration (secant method) and proceed according to the following algorithm:

1. First we assemble the global secant stiffness matrix $\mathbf{K}$ using, for every finite element, the nonlocal material compliance matrix $\mathbf{C}'$ (Eq. 10) which was obtained either in the preceding step (for the first iteration of this step) or in the previous iteration (for the subsequent iterations). In the first loading step, $\mathbf{C}'$ is the elastic compliance matrix of the material. Considering the load and displacement increments prescribed for this loading step, we solve the column matrix $\Delta\mathbf{u}$ of the nodal displacement increments and calculate $\mathbf{u}^F = \mathbf{u}^I + \Delta\mathbf{u}$ where F and I are the labels for the initial and final values in the loading step. Then we calculate $\boldsymbol{\epsilon}^F$ for all of the integration points of all finite elements. For each integration point we check whether cracking (damage) has started. If not, we calculate for this point the local coordinate direction x_1' (angle α) as the direction of the maximum principal strain ϵ_{11}^F. Otherwise we keep the old direction x_1'. Then we transform $\boldsymbol{\epsilon}^F$ into $\boldsymbol{\epsilon}'^F$ for the local coordinate.

2. With the help of a spatial averaging subroutine which approximates the integrals in Eqs. 6 and 7 by finite sums over the integration points, we calculate the nonlocal principal strains $\bar{\epsilon}_{11}^F$ and evaluate $(1 - \bar{\omega})^{-1}$ for all of the integration points of all elements (Eq. 9). Then we update matrices $\mathbf{C}'$ and $\mathbf{D}'$ and calculate the final stresses, $\boldsymbol{\sigma}'^F = \mathbf{D}'\boldsymbol{\epsilon}'^F$. This yields for each integration point of each

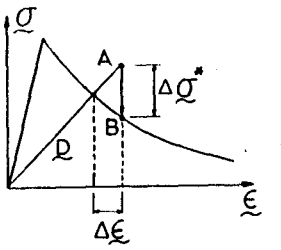

FIG. 3. Adjustment of Stress State (from point A to point B) to Stress–Strain Curve, as Implemented in Iteration of Loading Step

element the stress state corresponding to point B in Fig. 3 (in which point A shows the stress state based on the initial $\mathbf{C}'$ for this step). This stress state now satisfies the constitutive equations exactly but is not exactly in equilibrium with the loads because $\Delta\mathbf{u}$ was solved in step 1 on the basis of the old $\mathbf{C}'$ rather than the newly calculated $\mathbf{C}'$ (the initial equilibrium state is shown as point A in Fig. 3). Then we calculate the equivalent nodal forces $\mathbf{f}^E$ from $\boldsymbol{\sigma}'^F$ according to the principle of virtual work and evaluate the residual nodal forces $\mathbf{f}^R$ as $\mathbf{f}^R = \mathbf{f}^F - \mathbf{f}^E$ where $\mathbf{f}^F$ are the applied final nodal forces.

3. If the ratio $\Sigma|\mathbf{f}^R|/\Sigma|\mathbf{f}|$ is not less than a certain prescribed tolerance (for which the value 0.5% was used), then we return to step 1 and start the next iteration of this loading step. Otherwise we start at step 1 the first iteration of the next loading step.

Alternative II. Nonlocal Model with Rotating Smeared Cracks

The practice of keeping the crack direction constant and not allowing new cracks to form at oblique angles with this direction (as done in step 2 despite a possible rotation of the principal strain direction) is standard in the classical smeared cracking approach although not quite realistic. Recently, a better agreement with some measurements on cracked reinforced concrete panels (Gupta and Akbar 1984) has been obtained under the assumption that the cracks are always normal to the maximum principal strain, ϵ_1, and rotate as ϵ_1 rotates.

Although the hypothesis that the cracks rotate would be physically inadmissible if taken literally (Bažant 1983), it might nevertheless describe adequately a situation where the cracks of one direction close (and lock in shear) while cracks of another direction form. The main appeal of this hypothesis, however, is its simplicity.

A general smeared cracking model based on the assumption of rotating cracks has apparently not yet been formulated, and we will do so now, formulating it in a nonlocal form. We work now in Cartesian coordinates x_1, x_2 of fixed directions and denote as n_i the direction cosines of the current unit normal $\mathbf{n}$ to the crack planes. As already implied in Eq. 1, we consider the fracture strain (cracking strain) ϵ_{ij}^f to be a uniaxial strain. This means we assume the formation of cracks to affect neither the normal strains in the directions normal to $\mathbf{n}$ nor the shear strains on the crack plane. Therefore, the total stress–strain relation and the nonlocal cracking strain are:

$$\epsilon_{ij} = C_{ijkm}\sigma_{km} + \bar{\epsilon}^f_{ij}; \qquad \bar{\epsilon}^f_{ij} = n_i n_j \bar{\epsilon}^f \quad (11)$$

where $\bar{\epsilon}^f$ = nonlocal fracture strain magnitude and C_{ijkm} = initial elastic compliance tensor, which is isotropic and for two dimensions is the same as defined in Eq. 1 (with $\beta = 1$). Generally, for three dimensions, $C_{ijkm} = [(1 + \nu)(\delta_{ik}\delta_{jm} + \delta_{im}\delta_{jk}) - 2\nu\delta_{ij}\delta_{km}]/2E$.

For nonrotating cracks, Eq. 11 must coincide with Eq. 10. Therefore, if we set $\mathbf{n} = (1,0,0)$, we must have:

$$\frac{C_{1111}}{1 - \bar{\omega}}\sigma_{11} = C_{1111}\sigma_{11} + \bar{\epsilon}^f \quad (12)$$

From this we obtain $\bar{\epsilon}^f = [\bar{\omega}/(1 - \bar{\omega})]C_{1111}\sigma_{11}$ where $C_{1111} = 1/E'$; $E' = E$ for plane stress as well as for three dimensions. Noting that $\sigma_{11} = n_1 n_1 \sigma_{11}$, we obtain for a general crack direction the generalization:

$$\bar{\epsilon}^f = \frac{\bar{\omega}}{(1 - \bar{\omega})\,E'} n_k n_m \sigma_{km} \quad (13)$$

Thus the total stress–strain relation for Alternative II is:

$$\epsilon_{ij} = \left[C_{ijkm} + \frac{\bar{\omega}}{(1 - \bar{\omega})E'} n_i n_j n_k n_m\right]\sigma_{km} \quad (14)$$

as recently proposed by Bažant. The bracketed term represents the secant compliance tensor. Note that, for loading, $\bar{\omega}/(1 - \bar{\omega}) = \phi(\bar{\epsilon}_f)$, because of Eq. 9; $\bar{\epsilon}_f$ is the nonlocal maximum principal strain; $\epsilon_f = n_i n_j \epsilon_{ij}$. Here we imply again the assumption that the orientation of cracks is decided by the principal direction n_i of nonlocal strain $\bar{\epsilon}_{ij}$ rather than the local strain ϵ_{ij}. The vector $\mathbf{n}$ in general rotates and must be evaluated at each stage of computation for each integration point of each finite element.

The computational algorithm is analogous to that we described for Alternative I but simpler in that one need not keep track of the coordinate axes for cracking at each integration point and need not carry out the corresponding rotation transformations. The finite-element results for the example that follows happen to be almost exactly the same because the principal stress directions remain nearly constant in this fracture test.

The decision in favor of Alternative I or II will necessitate further testing, since at present there apparently exist no test data for strain softening (progressive fracture) of plain concrete at rotating principal stress directions. A fully realistic model no doubt calls for allowing partial or full cracking in all directions, as is done in the microplane model (Bažant and Prat 1988).

It should be pointed out that function ϕ might depend separately on the average, ϵ_L, of the lateral normal strains in the directions normal to $\mathbf{n}$; $\epsilon_L = (\epsilon_{II} + \epsilon_{III})/2 = (\epsilon_{kk} - n_i n_j \epsilon_{ij})/2$. The reason is that compressive lateral stresses alone can produce axial splitting cracks, as known for example from the uniaxial compression test. However, they also produce tensile strain ϵ_t, and thus it might be that the dependence of ϕ on $\bar{\epsilon}_f$ approximately accounts for the compression splitting cracks as well. Further study and testing is needed.

Fracture Specimens and Size Effect Due to Nonlocal Aspect

Without a nonlocal formulation, the finite-element codes with strain softening cannot describe the results of fracture tests. In particular, such finite-element codes yield no size effect. Yet the size effect is the principal, experimentally verified feature of fracture mechanics.

To demonstrate that the nonlocal smeared crack model correctly describes fracture and especially the size effect, we analyze the three-point-bend specimens shown in Fig. 4. Three different specimen sizes of size ratios 1:2:4, with geometrically similar shapes, were considered. Their finite element meshes are shown in Fig. 5 and their refinements in Fig. 6. The problem was solved both for linear strain softening and exponential strain softening, shown in Fig. 7.

This type of specimen was tested at Northwestern University (Bažant and Pfeiffer 1987), using both concrete with maximum aggregate size $d_a = 0.5$ in. (12.7 mm) and mortar with $d_a = 0.19$ in. (4.83 mm). The maximum loads P were measured for each specimen of each size, from which the values of the nominal stress at failure σ_N were calculated; $\sigma_N = P/bd$ where b = specimen thickness (1.5 in. or 38.1 mm). The test results are shown in

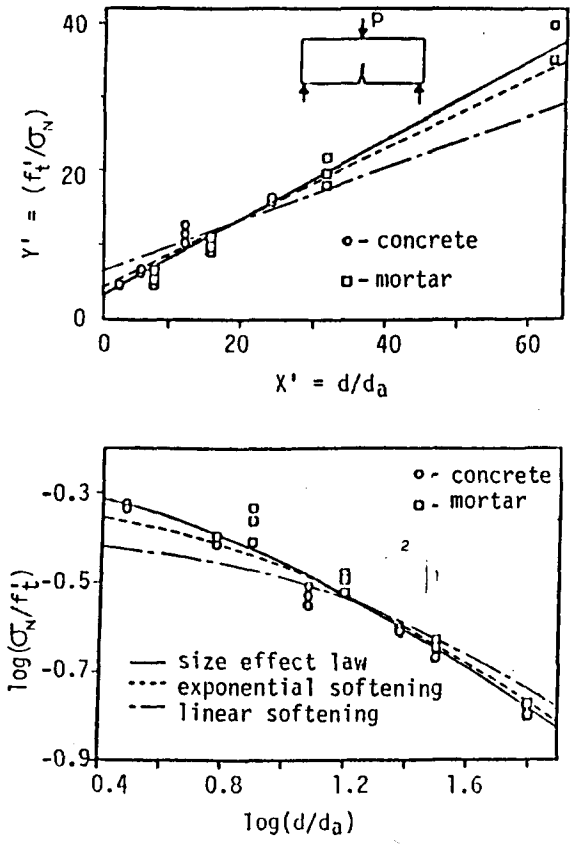

FIG. 4. Test Results of Bažant and Pfeiffer (1987) in Size Effect Plot (bottom) and Linear Regression Plot (top) Compared to Size Effect Law as Well as to Finite-Element Results for Linear and Exponential Strain Softening (Three-Point-Bent Specimen)

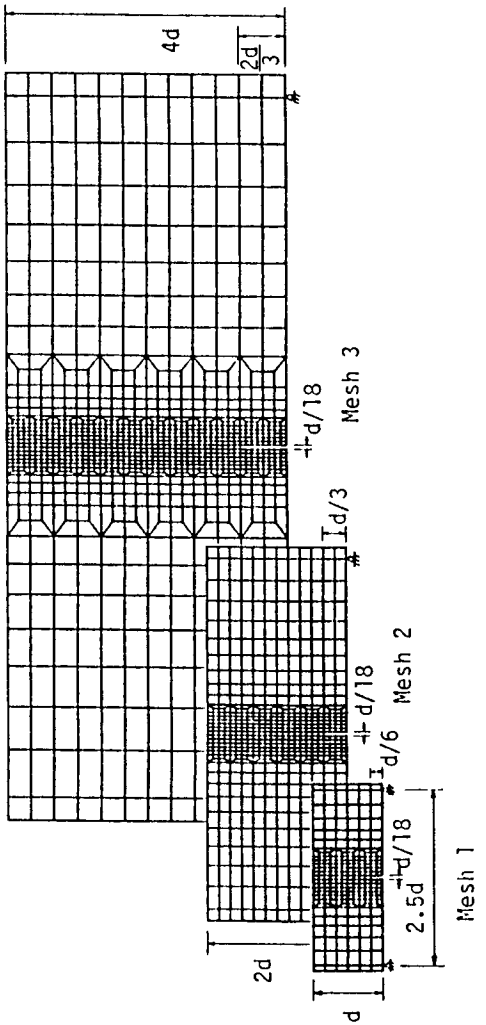

FIG. 5. Finite-element Meshes Used for Nonlocal Analysis of Specimens of Three Sizes

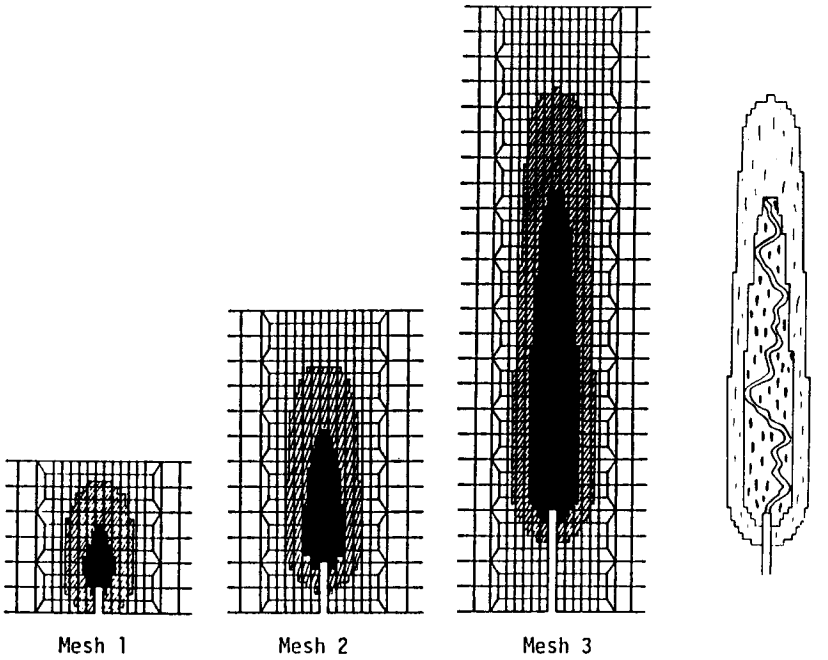

FIG. 6. Extents of Softening Zone (cross-hatched) and Fracture Zone (black) Obtained by Nonlocal Finite-Element Analysis

Fig. 4 in the size effect plots (bottom) and the corresponding linear regression plots (top), where f_t' = direct tensile strength of concrete. The solid lines in this figure represent the optimum fit of these test results with Bažant's size effect law for blunt fracture (Bažant 1984; Bažant and Pfeiffer 1987):

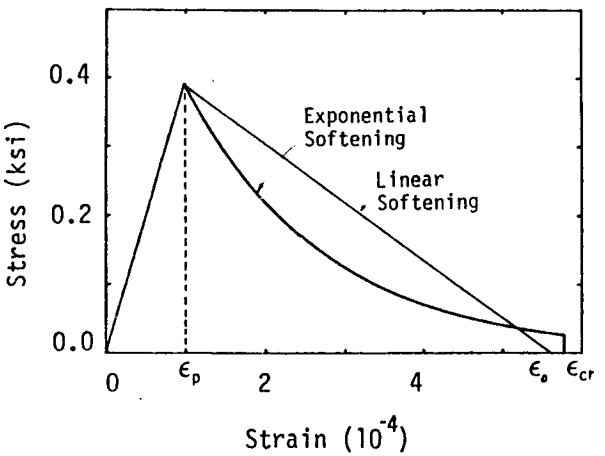

FIG. 7. Stress–Strain Diagram Used in Nonlocal Finite-Element Analysis

$$\sigma_N = Bf'_t \left[1 + \left(\frac{d}{\lambda_0 d_a} \right)^r \right]^{-1/2r} \qquad (15)$$

in which the coefficient r may be approximately taken as 1, and B and λ_0 are two empirical constants which can be determined from the test data in Fig. 4. To this end, Eq. 15 may be algebraically rearranged to the linear regression equation $Y = AX + C$, in which $X = (d/d_a)^r$, $Y = (f'_t/\sigma_N)^{2r}$, $C = B^{-2r}$, and $A = C\lambda_0^{-r}$. The linear regression plots, shown for the measured data in Fig. 4 [taken from Bažant and Pfeiffer (1987)], yield the coefficients B and λ_0 from the slope A and the Y-axis intercept C. Furthermore, E = 3976 ksi (27420 MPa), $\nu = 0.18$, and f'_t = 390 psi (2.69 MPa). The remaining material parameters were determined so as to obtain with the finite-element program and the meshes in Figs. 5 and 6 optimum fits of the test data in Fig. 4. These values were, for the linear strain softening, $E_t = -726$ ksi (-5007 MPa), and l = 2.3 in. (58.42 mm), and for the exponential strain softening, c = 690 psi (4.76 MPa), a = 5730 psi (39.52 MPa), l = 3.2 in. (81.28 mm). The corresponding optimum values of the fracture energy were G_f = 0.230 lb/in. (40.29 N/m) for the linear strain softening, and 0.249 lb/in. (43.62 N/m) for the exponential strain softening.

The fracture energy is equal to the area under the stress–strain diagram in Fig. 7 times the effective width of the fracture process zone, w_c. The value of w_c for the classical (local) crack band model is defined clearly; it coincides with the width of the crack band or the size of the finite element. But w_c is harder to define for the nonlocal formulation since the effective width of the fracture process zone varies (Fig. 6), depending on the influence of the boundaries and other factors. The actual width of the fracture process zone is roughly equal to 2.7 l (Bažant and Pijaudier-Cabot 1988), but since the density of cracking decreases from the middle of the crack band to its boundary, the effective width of the fracture process zone based on uniform distribution of the energy dissipation (or of cracking density) is about l. The aforementioned values of G_f correspond to the area under the stress–strain diagram times l.

The most important test to determine whether the finite-element model correctly describes fracture is the size effect. For structures that follow the strength criterion (or yield criterion), there is no size effect, i.e., the plot in Fig. 4 is represented by a horizontal line. The linear elastic fracture mechanics yields the strongest possible size effect which corresponds to the straight inclined line of slope $-1/2$ shown in Fig. 4 (bottom). For materials that exhibit distributed cracking, the size effect plot represents a smooth transition from the horizontal line for the strength criterion to the inclined straight line for the linear elastic fracture mechanics, as shown in Fig. 4 (bottom).

The load-displacement curves calculated by the nonlocal finite-element program for the three meshes shown in Figs. 5 and 6 are plotted in Fig. 8. The maximum load values, P_{max}, were fitted by the size effect law (Eq. 15), for which A = 0.384, C = 6.169 for the linear strain softening, and A = 0.483, C = 3.971 for the exponential strain softening. The agreement with the size effect law was rather accurate, with the error (deviation from Eq. 15) not exceeding 5%. The curves of the size effect law (Eq. 15), which were obtained by the optimum fits of the values of P_{max} calculated by finite elements for the three specimen sizes, are shown in Fig. 4 as the dashed

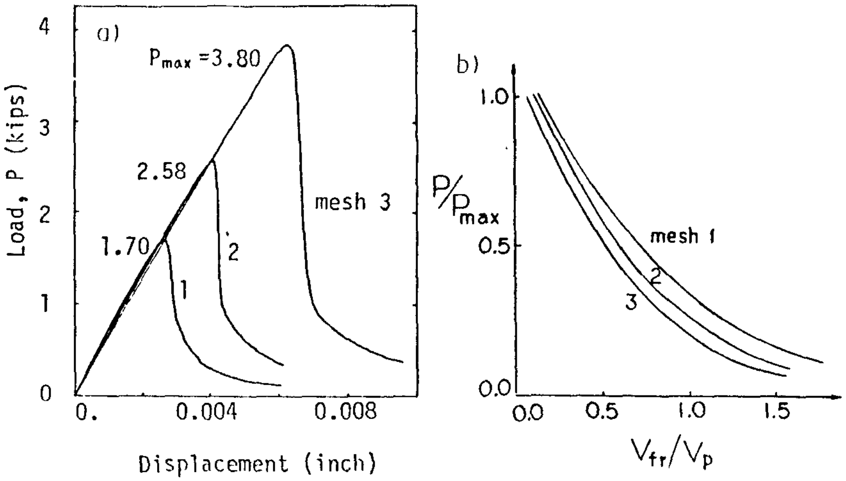

FIG. 8. (a) Diagrams of Load Versus Load-Point Displacement for Three-Point-Bend Specimens of Three Sizes Obtained with Meshes in Figs. 5 and 6; (b) Corresponding Diagrams of Load Versus Load-Point Fracture Displacement

lines for the exponential strain softening and the dash–dot lines for the linear strain softening.

An interesting feature is now noticed from Fig. 4: the shape of the strain-softening diagram significantly influences the shape of the size effect curve. This fact has already been noticed in other studies for different reasons. Evidently, the exponential strain softening agrees with the test results much better than the linear strain softening, which was originally used in the crack band model (Bažant and Oh).

Another interesting plot is that of load P versus the part, v_{fr}, of the load-point displacement v that is due to fracture and is defined as $v_{fr} = v - C_e P$, in which C_e is the elastic compliance of the specimens associated with load P. The plots of P versus displacement for the three specimen sizes and three finite-element meshes are shown in Fig. 8(a). We see that, for increasing specimen size, the initial postpeak drop of the load gets larger and larger (v_p = load-point displacement at maximum load). This indicates an increasing brittleness of the specimen as its size increases, in accordance with the size effect law.

If the presently considered specimens of three different sizes are analyzed with geometrically similar meshes using the classical (local) smeared cracking model based on the strength criterion, the resulting maximum load values show no size effect, i.e. the plot in Fig. 4 is horizontal. Thus, the classical smeared cracking is incapable of describing the size effect. This is obviously unsatisfactory, in contradiction to fracture tests as well as tests of various brittle failures of concrete structures. On the other hand, if these three specimen sizes are analyzed by a finite-element code for linear elastic fracture mechanics, the results match the straight line of slope $-1/2$ shown in Fig. 4 (bottom), for which the size effect is too strong.

Fig. 6 shows for the three specimen sizes and the corresponding meshes the extent of the strain-softening zone (cross-hatched area) and of the fully

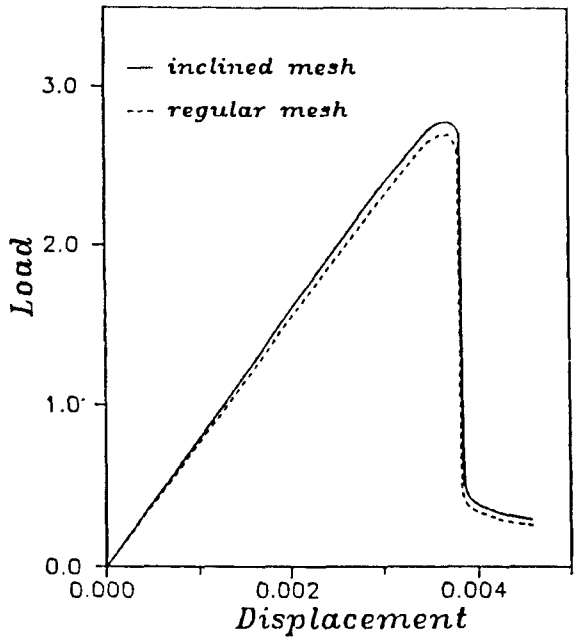

FIG. 9. Load Versus Load-Point Displacement Diagram Obtained for Three-Point-Bent Specimen for Orthogonal and Slanted Meshes Shown in Fig. 10.

fractured zone (black area). The former zone is defined as the locus of the material states for which the peak-stress point has been passed (i.e., $\epsilon_{11} > \epsilon_p$), and the latter zone is defined as the zone for which the stress σ_{11} has been reduced to less than $0.06\sigma_p$.

It should be kept in mind that normally the final fracture surface is not plane but highly tortuous. As an approximation, it may be assumed that the final crack surface randomly meanders through the black zone, oscillating on its way between the zone boundaries (Fig. 6, right). The resolution that can be obtained with the nonlocal model for element sizes that are much smaller than the aggregate size is of course meaningful only in a statistical sense since on such a scale the material behavior is highly random. The boundaries of the zones in Fig. 6, as well as the stress and strain values obtained for the fine meshes shown, must be regarded as merely statistical averages which correspond to smoothing of the random fields of microstresses and microstrains, and to averaging over a large number of tests of statistically identical specimens. The black zone corresponds to dense microcracking (normally invisible to the eye) and the strain-softening zone to sparse microcracking (Fig. 6, right).

The results shown in Fig. 6 for the three meshes have another interesting implication: the width of the fracture process zone as well as the softening zone is not constant but varies. In consequence, the rate of energy dissipation per unit fracture extension is variable, too. To capture such variation might be one important purpose of refining the mesh, possibly even below the aggregate size.

As a further implication, the present nonlocal model does not correspond to a unique stress-displacement diagram if the strain across the softening band is lumped into a crack opening displacement, equivalent to that used in models of Hillerborg's type. Rather, the equivalent discrete crack model would have to use somewhat different stress-displacement softening diagrams depending on the distance of the fracture front from the notch and from the specimen boundaries.

The computer running times for the nonlocal analyses are usually shorter than for the corresponding local analyses. Apparently, the additional computer time needed to calculate the spatial averages over the mesh is more than offset by improvement of the convergence of iterations, due to the stabilizing influence of the nonlocal formulation.

For other types of nonlocal continuum with local elastic strain, convergence at mesh refinement has been demonstrated before (Bažant et al. 1987; Bažant and Pijaudier-Cabot 1987, 1988; Pijaudier-Cabot and Bažant 1987). The fact that, despite mesh refinement, the energy dissipation cannot localize in these nonlocal models into a zone of zero volume has also been mathematically proven in general (Bažant and Pijaudier-Cabot 1987, 1988).

Elimination of Directional Bias of Mesh

With the crack band model in which the strain-softening band is one element wide, it has been difficult to simulate fractures that propagate at a small angle ϕ with regard to the mesh line, although some artificial measures (Pan

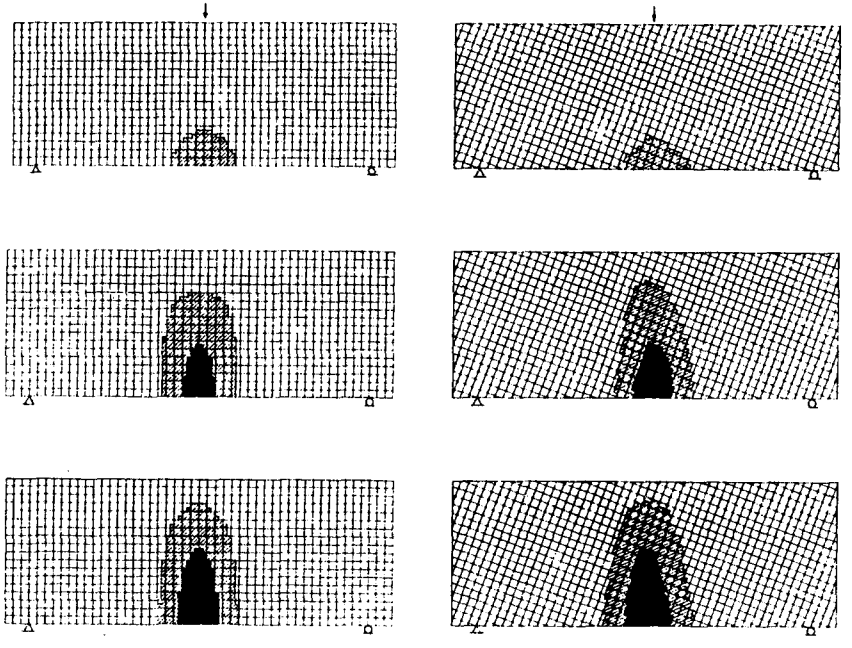

FIG. 10. Orthogonal Mesh and Slanted Mesh Used in Nonlocal Finite-Element Analyses, with Softening and Fracture Zones Obtained in Both Cases

et al. 1984) were found to offer partial help. To study this aspect, the presently considered specimen of the smallest size has been analyzed by finite elements using the slanted square mesh shown in Fig. 10 (right), whose inclination is 20°. The softening and fracture zones obtained are shown in Fig. 10 on the left for the orthogonal mesh and on the right for the slanted mesh. Success is now noticeable. The zone boundaries obtained for the orthogonal and slanted meshes are nearly the same, and the propagation for the slanted mesh still occurs in the correct vertical direction.

The problem of simulating propagation of crack bands in directions inclined with regard to the mesh line has recently been studied by Droz (1987) and for the analogous problem of shear bands by Leroy and Ortiz (1988). (The classical approach, in which the smeared cracking or the shear band tends to localize into a band of single-element width, fails since a localization limiter such as the nonlocal continuum concept cannot be used.) These investigators achieved propagation in oblique directions by superimposing on a continuous displacement field of the finite elements a certain additional discontinuous field which simulates the discontinuity of the zig-zag crack or shear band running in an inclined direction. However, the programming of this approach for general finite-element programs seems to be quite difficult. By contrast, the present approach is quite simple, although it does require mesh refinements such that there are at least three finite elements across the width of the cracking band. The present approach could also be adopted for the modeling of inclined shear bands.

Conclusions

1. The well-known inobjectivity, spurious mesh sensitivity, and incorrect convergence of the classical smeared cracking model can be eliminated by adopting a nonlocal formulation in which cracking (or strain softening) is characterized by nonlocal damage. The nonlocal damage may be considered to be a function of the spatial average of the positive part of the maximum principal strain. The nonsoftening (elastic) response is treated as local.

2. The finite-element results closely agree with the results of fracture tests, in particular with the observed influence of specimen size on the maximum load, which is described by Bažant's size effect law.

3. The nonlocal approach eliminates the directional bias of the mesh, provided the mesh is sufficiently refined. In particular, the results obtained with orthogonal and slanted meshes give approximately the same direction of fracture propagation and the same boundaries of the strain-softening zone and the fracture zone.

4. The nonlocal model is numerically efficient and easily programmed. It merely requires introducing into an existing code a subroutine for the spatial averaging of the maximum principal strains.

5. The nonlocal smeared model is formulated in two alternatives: the classical one in which the crack direction is fixed when the cracking starts, and a novel one in which the cracks are imagined to rotate along with the maximum principal strain direction. The latter alternative is simpler.

Acknowledgment

Partial financial support for the general nonlocal concept has been obtained under AFOSR contract No. F49620-87-C-0030DEF with Northwestern University, monitored by Dr. Spencer T. Wu, and for the detailed formulation and finite-element programming under NSF Grant MSM-9877830 to Northwestern University. Supercomputer funds (on CRAY X-MP/48) were provided under NSF Grant 00000-MSM8211642.

Appendix. References

Bažant, Z. P. (1976). "Instability, ductility and size effect in strain-softening concrete." *J. Engrg. Mech.*, ASCE, 102(2), 331–344. Discussions, 103, 357–358, 775–777; 104, 501–502 (based on *Struct. Engrg. Report No. 74-8/640*, Northwestern University, August 1974).

Bažant, Z. P. (1983). "Comment on orthotropic models for concrete and geomaterials." *J. Engrg. Mech.*, ASCE, 109(3), 849–865.

Bažant, Z. P. (1984). "Size effect in blunt fracture: Concrete, Rock, Metal." *J. Engrg. Mech.*, ASCE, 110(4), 518–535.

Bažant, Z. P. (1986). "Mechanics of distributed cracking." *Appl. Mech. Rev.*, ASME, 39(5), 675–705.

Bažant, Z. P. (1987). "Snapback instability at crack ligament tearing and its implication for fracture micromechanics." *Cement and Concrete Res.*, 17(6), 951–967.

Bažant, Z. P., Belytschko, T. B., and Chang, T. P. (1984). "Continuum theory for strain-softening." *J. Engrg. Mech.*, ASCE, 110(12), 1666–1692.

Bažant, Z. P., and Cedolin, L. (1979). "Blunt crack band propagation in finite element analysis." *J. Engrg. Mech.*, ASCE, 105(2), 297–315.

Bažant, Z. P., and Cedolin, L. (1980). "Fracture mechanics of reinforced concrete. *J. Engrg. Mech.*, ASCE, 106(6), 1287–1306. Discussion and Closure (1982), 108, 464–471.

Bažant, Z. P., and Gambarova, P. (1981). "Rough cracks in reinforced concrete." *J. Struct. Engrg.*, ASCE, 106(4), 819–842. Discussions and Closure, 2579–2581, 1377–1388

Bažant, Z. P., Lin, F. B., and Pijaudier-Cabot G. (1987). "Yield limit degradation: Nonlocal continuum model with local strain." Preprints, *Int. Conf. On Computational Plasticity*, held in Barcelona, D. R. J. Owen, E. Hinton, and E. Onate, eds. Univ. of Wales, Swansea, 1757–1780.

Bažant, Z. P., and Oh, B. H. (1983). "Crack band theory for fracture of concrete." *Materials and Structures*, RILEM, Paris, France, 16, 155–177.

Bažant, Z. P., and Oh, B. H. (1984). "Rock fracture via strain-softening finite elements." *J. Engrg. Mech.*, ASCE, 110(7), 1015–1035.

Bažant, Z. P., and Pfeiffer, P. A. (1987). "Determination of fracture energy from size effect and brittleness number." *ACI Mat. J.* 84 (Nov.–Dec.), 463–480.

Bažant, Z. P., and Pijaudier-Cabot, G. (1987). "Modeling of distributed damage by nonlocal continuum with local strain." Preprints. *4th Intern. Conf. on Numerical Methods in Fracture Mechanics*, A. R. Luxmore, D. R. J. Owen, and M. F. Kanninen, eds., held in San Antonio, Texas, Mar., 411–432.

Bažant, Z. P., and Pijaudier-Cabot, G. (1988). "Nonlocal continuum damage, localization instability and convergence." *J. Appl. Mech.*, ASME, 55(June), 287–293.

Bažant, Z. P., and Prat, P. C. (1988). "Microplane model for brittle-plastic material—I. Theory, II. Verification." *J. Engrg. Mech.*, ASCE, 114(10), 1672–1702.

Cedolin, L., and Bažant, Z. P. (1980). "Effects of finite element choice in blunt crack band analysis." *Computer Methods in Appl. Mech. and Engrg.* 24(3), 305–316.

Darwin, D. (1985). "Concrete crack propagation—Study of model parameters." *Proc. Finite Element Analysis of Reinforced Concrete Structures*. C. Meyer and H. Okamura, eds. ASCE, New York, 184–203.

De Borst, R. (1984). "Application of advanced solution techniques to concrete cracking and non-associated plasticity." *Numerical methods for non-linear problems*, C. Taylor et al., eds. Vol. 2, Pineridge Press, Swansea, United Kingdom, 314–325.

De Borst, R, and Nauta, P. (1984). "Smeared crack analysis of reinforced concrete beams and slabs failing in shear." *Proc. Int. Conf. on Computer-aided Analysis and Design of Concrete Structures*, Split, Yugoslavia, 261–274.
De Borst, R., and Nauta, P. (1985). "Non-orthogonal cracks in a smeared finite element model." *Eng. Computation*, 2, 35–46.
Droz, P. (1987). "Numerical modeling of the non-linear behavior of massive structures of unreinforced concrete," doctoral thesis No. 682, Ecole Polytéchnique Fédérale de Lausanne, Switzerland.
Eringen, A. C., and Edelen, D. G. B. (1972). "On nonlocal elasticity." *Int. J. Eng. Sci.*, No. 10, 233–248.
"Finite element analysis of reinforced concrete." (1982). *State of the Art Report*, prepared by Task Committees, chaired by A. H. Nilson, ASCE, New York, Chapter 4, 204–233.
Gupta, A. K. and Akbar, H. (1984). "Cracking in reinforced concrete analysis." *J. Struct. Engrg.*, ASCE, 110(8), 1735.
Hand, F. R., Pecknold, D. A., and Schnobrich, W. C. (1973). "Nonlinear layered analysis of RC plates and shells, *J. Struct. Engrg.*, ASCE, 99(7), 1491–1505.
Hillerborg, A. (1985). "Numerical methods to simulate softening and fracture of concrete." *Fracture mechanics of concrete: Structural application and numerical calculation*, G. C. Sih and A. DiTomasso, eds. Martinus Nijhoff, Doordrecht–Boston, 141–170.
Hillerborg, A., Modéer, M., and Petersson, P. E. (1976). "Analysis of crack formation and crack growth in concrete by means of fracture mechanics and finite elements." *Cement and Concrete Res.* 6(6), 773–782.
Ingraffea, A. (1985). "Fracture propagation in rock." *Mechanics of geomaterials: Rocks, concretes, soils*, Z. P. Bažant, ed. John Wiley and Sons, Inc., New York, N.Y., 219–258.
Ingraffea, A. R., and Saouma, V. (1985). "Numerical modeling of discrete crack propagation in reinforced and plain concrete." *Fracture mechanics of concrete: Structural application and numerical calculation*, G. C. Sih and A. DiTomasso, eds. Martinus Nijhoff, Doordrecht–Boston, 171–225.
Leroy, Y., and Ortiz, M. (1988). "Finite element analysis of strain localization in frictional materials." Report, Div. of Engrg., Brown Univ., Providence, R.I.
Lin, C.-S., and Scordelis A. (1975). "Nonlinear analysis of RC shells of general form." *J. Struct. Engrg.*, ASCE, 101(3), 523–538.
Marchertas, A. H., Kulak, R. F., and Pan, Y. C. (1982). "Performance of blunt crack approach within a general purpose code." *Nonlinear numerical analysis of reinforced concrete*, L. E. Schwer, ed. ASME, New York; N.Y., 107–123.
Ngo, D., and Scordelis A. C. (1967). "Finite element analysis of reinforced concrete beams." *ACI J.* 64(3), 152–163.
Pan, Y. C., Marchertas, A. H., and Kennedy, J. M. (1983). "Finite element analysis of blunt crack propagation, a modified J-integral approach." *Trans. 7th Int. Conf. on Structural Mechanics in Reactor Technology*, Paper H5/3, North-Holland, Amsterdam, 235–292.
Pan, Y. C., Marchertas, A. H., Pfeiffer, P. A., and Kennedy, J. M. (1984). "Concrete cracking simulations for nuclear applications." *Theoret. Appl. Fracture Mech.*, 2(1), 27–38.
Pijaudier-Cabot, G., and Bažant, Z. P. (1986). "Nonlocal damage theory." *Report No. 86-8/428n*, Center for Concrete and Geomaterials, Northwestern Univ., Evanston, Ill.
Pijaudier-Cabot, G., and Bažant, Z. P. (1987). "Nonlocal damage theory." *J. Engrg. Mech.*, ASCE, 113(10). 1512–1533.
Rashid, Y. R. (1968). "Analysis of prestressed concrete pressure vessels." *Nuclear Engrg. and Design* 7(4), 334–355.
Suidan, M., and Schnobrich, W. C. (1973). "Finite element analysis of reinforced concrete." *J. Struct. Engrg.*, ASCE, 99(10), 2109–2122.
Yuzugullu, O., and Schnobrich, W. C. (1973). "A numerical procedure for the determination of the behavior of a shear wall frame system." *ACI. J.* 70(7), 474–479.